Journal of Molecular Structure 1036 (2013) 161–167

Contents lists available at SciVerse ScienceDirect

Journal of Molecular Structure

journal homepage: www.elsevier.com/locate/molstruc

New zinc(II), palladium(II) and platinum(II) complexes of DL-piperidine-2-carboxylic acid; X-ray crystal structure of *trans*-$[Zn_2(\mu\text{-}Ca)_2(Hpa)_2Cl_6]$ and anticancer activity of some complexes

Afaf A. Alie El-Deen [a], Abd El-Monem E. El-Askalany [a], Ruba Halaoui [b], Bertrand J. Jean-Claude [b], Ian S. Butler [c], Sahar I. Mostafa [a,*]

[a] *Chemistry Department, Faculty of Science, Mansoura University, Egypt*
[b] *Royal Victoria Hospital, Department of Medicine, Montreal, QC, Canada H3A 1A1*
[c] *Department of Chemistry, McGill University, Montreal, QC, Canada H3A 2K6*

HIGHLIGHTS

- We prepared and characterized new complexes of DL-piperidine-2-carboxylic acid (H_2pa).
- The addition of $ZnCl_2$ to DL-H_2pa in either hard tap water or in presence of $CaCl_2$, obtained *trans*-$[Zn_2(m\text{-}Ca)_2(Hpa)_2Cl_6]$.
- The X-ray structure of *trans*-$[Zn_2(m\text{-}Ca)_2(Hpa)_2Cl_6]$ shows two $Zn(Hpa^-)Cl_3$ units (each zinc atom ligates by carboxyl oxygen and three chlorine atoms) bridged by two calcium atoms.
- The free DL-H_2pa and its complexes, *trans*-$[Zn_2(m\text{-}Ca)_2(Hpa)_2Cl_6]$, [Pd(bpy)(Hpa)]Cl and $[M(pa)(PPh_3)_2]$ (M(II) = Pd, Pt) have been tested against the serous ovarian cancer ascites, OV90 cell line in comparison to cis-platin.
- $[Pt(PPh_3)_2(pa)]$ exhibits the highest growth inhibitory activity with mean IC50 43.13 μM.

ARTICLE INFO

Article history:
Received 20 June 2012
Received in revised form 14 September 2012
Accepted 17 September 2012
Available online 26 September 2012

Keywords:
Palladium
Zinc
DL-piperidine-2-carboxylic acid
Platinum
Anticancer

ABSTRACT

New complexes of DL-piperidine-2-carboxylic acid (DL-H_2pa), $[Zn(Hpa)(AcO)(H_2O)_2]$, *trans*-$[Zn_2(\mu\text{-}Ca)_2(Hpa)_2Cl_6]$, $[M(bpy)(Hpa)]Cl$ and $[M(pa)(PPh_3)_2]$ (M(II) = Pd, Pt) have been prepared and characterized on the basis of elemental analyses, molar conductivity and thermal measurements, IR, Raman, UV–Vis, NMR (^1H and ^{31}P) and mass spectroscopy. DL-Piperidine-2-carboxylic acids act as bidentate ligands, through the carboxyl oxygen and cyclic nitrogen atoms. The crystal structure of *trans*-$[Zn_2(\mu\text{-}Ca)_2(Hpa)_2Cl_6]$, obtained from the addition of $ZnCl_2$ to DL-H_2pa in either hard tap water or presence of $CaCl_2$, has been determined by X-ray diffraction. It crystallizes in a triclinic lattice with space group symmetry P1. The complex has two zinc atoms in tetrahedral geometry, each ligated by a carboxyl oxygen and three chlorine atoms. The other carboxyl oxygen atoms from the two Hpa^- ligands are bridged by two calcium atoms, i.e., there are two $Zn(Hpa^-)Cl_3$ units bridged by two calcium atoms. The free DL-H_2pa and its complexes, *trans*-$[Zn_2(\mu\text{-}Ca)_2(Hpa)_2Cl_6]$, [Pd(bpy)(Hpa)]Cl and $[M(pa)(PPh_3)_2]$ (M(II) = Pd, Pt) have been tested against the serous ovarian cancer ascites, OV 90 cell line.

1. Introduction

Piperidine-2-carboxylic acid is known as a pharmaceutically active compound [1]. The spectral data support its presence in a Zwitterionic form, similar to common amino acids [2]. Over the past few years, our laboratory has been actively involved in the synthesis of various transition metal complexes of piperidine-2-carboxylic acid [3]. Some of these complexes have been evaluated as anticancer agents against *Ehrlich ascites* tumor cells (EACs) [3]. Inomata et al. [4–6] have reported number of complexes with piperidine-2-carboxylic acid (pipe-2), piperidine-3-carboxylic acid (pipe-3) and piperidine-4-carboxylic acid (pipe-4). Also, the X-ray crystal structures of the complexes, $[Cu(pipe\text{-}2)_2(H_2O)_2]$ [7], $[CdCl_2(\text{D-Hpipe-2})(H_2O)]$–$[CdCl_2(\text{L-Hpipe-2})(H_2O)]$, have been published [4].

In continuation of our search for potent active anticancer complexes, it was considered worthwhile to synthesize new complexes of DL-piperidine-2-carboxylic acid (DL-H_2pa) with Zn(II), Pd(II) and Pt(II). The structure of the resulting complexes have been investigated on the basis of elemental analyses and spectral (IR, Raman, UV–Vis, ^1HNMR, mass), thermal and molar conductivity measurements. The X-ray crystal structure of *trans*-$[Zn_2(\mu\text{-}Ca)_2(Hpa)_2Cl_6]$

* Corresponding author. Tel.: +20 100 8502625; fax: +20 50 2246781.
E-mail address: sihmostafa@yahoo.com (S.I. Mostafa).

0022-2860/$ - see front matter © 2012 Elsevier B.V. All rights reserved.
http://dx.doi.org/10.1016/j.molstruc.2012.09.045

have been also determined. The anticancer activity of DL-H_2pa and its complexes, *trans*-[$Zn_2(\mu\text{-}Ca)_2(Hpa)_2Cl_6$], [Pd(bpy)(Hpa)]Cl and [M(pa)(PPh_3)$_2$] (M(II) = Pd, Pt) have been tested against the serous ovarian cancer ascites, OV 90 cell line.

2. Experimental

2.1. Materials and measurements

All reagents and solvents were purchased from Alfa/Aesar and all manipulations were performed under aerobic conditions using materials and solvents as received. [M(PPh_3)$_2Cl_2$] and [M(bpy)Cl_2] (M(II) = Pd, Pt) were prepared by the literature methods [8,9]. DMSO-d_6 was used for the NMR measurements, which were referenced against TMS.

The human serous ovarian cancer ascites, OV 90 cell line was obtained from the American Type Culture Collection (ATCC catalog number). Cells were maintained in Dulbecco's Modified Eagle Medium (Wisent Inc., St-Bruno, Canada) supplemented with 10% FBS, 10 mM HEPES, 2 mM L-glutamine and 100 μg/mL penicillin/streptomycin (GibcoBRL, Gaithersburg, MD). In all assays cells were plated 24 h before drug treatment.

2.2. Instrumentation

Elemental analyses and X-ray crystallography were performed in the Department of Chemistry, Montreal University. The crystal structure was measured at the X-ray crystal structure unit, using a Bruker Platform diffractometer, equipped with a Bruker MART 4 K Charger-Coupled Device (CCD) Area Detector using the program APEX II and a Nonius Fr591 rotating anode (Copper radiation) equipped with Montel 200 optics. The crystal-to-detector distance was 5 cm and the data collection was carried out in 512 × 512 pixel mode. The initial unit cell parameters were determined by the least-squares fit of the angular setting of strong reflections, collected by a 10.0° scan in 33 frames over three different parts of the reciprocal space (99 frames total) and one complete sphere of data was collected. Infrared spectra were recorded on a Nicolet 6700 Diamond ATR spectrometer in the 4000–200 cm^{-1} range. Raman spectra were measured on an In-via Renishaw spectrometer using 785-nm laser excitation. NMR spectra were recorded on VNMRS 500-MHz spectrometer in DMSO-d_6 using TMS as reference. Mass spectra, ESI-MS and EI-MS were recorded using LCQ Duo and double-focusing MS25RFA instruments, respectively. Electronic spectra were measured in DMF using a Hewlett–Packard 8453 spectrophotometer. Thermal analysis studies were made in the 20–800 °C range at a heating rate of 20 °C min^{-1} using Ni and NiCo as references, on a TA instrument TGA model Q500Analyzer TGA-50. Molar conductivity measurements were carried out at room temperature on a YSI Model 32 conductivity bridge.

2.3. Preparations

2.3.1. [Zn(Hpa)(AcO)(H_2O)$_2$]

Zinc acetate (0.054 g, 0.25 mmol) in methanol (10 mL) was added to DL-H_2pa (0.032 g, 0.25 mmol) in methanol (10 mL). The reaction mixture was stirred for 4 h. Upon reducing the volume, a white precipitate was obtained, which was filtered off, washed with methanol and air-dried. Yield: 80%. Anal. Calcd. for $C_8H_{17}NO_6$-Zn: C, 33.3; H, 5.9; N, 4.9; Zn, 22.7%, Found: C, 33.2, H, 5.8; N, 5.0; Zn, 22.5%. Conductivity data (10^{-3} M in DMF): Λ_M = 10.0 ohm^{-1}. IR (cm^{-1}) ν(NH) 3125; $\nu_{as}(COO^-)$ 1625; $\nu_s(COO^-)$ 1369; δ(NH) 1560; ν(Zn—O) 510; ν(Zn—N) 470 cm^{-1}. Raman: $\nu_{as}(COO^-)$ 1632; $\nu_s(COO^-)$ 1410; δ(NH) 1540; ν(Zn—O) 532; ν(Zn—N) 410 cm^{-1}; ^{1}H NMR (d_6-DMSO/TMS, ppm), δ: 3.41 (d, 2H, Hα); 2.48 (m, 2H, Hβ); 2.03 (m, 2H, Hγ); 1.44 (m, 2H, Hδ); 3.21, 2.70 (m, 2H, Hε); 13.20 (s, 1H, NH), ESI-MS: *m/z*, 386.0 [Zn(Hpa)(AcO)(H_2O)$_2$]$^+$; 256.0 [Zn(Hpa)(AcO)]$^+$; 194.0 [Zn(Hpa)]$^+$; 178.0 [Zn(Hpa—O)]$^+$.

2.3.2. Trans-[$Zn_2(\mu\text{-}Ca)_2(Hpa)_2Cl_6$]·1/3$H_2O$

An aqueous solution of zinc chloride (0.136 g, 1 mmol; 15 mL) was added to an aqueous solution of DL-H_2pa (0.129 g, 1 mmol; 15 mL). The resulting solution was stirred with gentle heating for 5 h. Upon reducing the volume, white crystals separated out. These were filtered off, washed with water and dried *in vacuo*. Yield: 65%. Anal. Calcd. for $C_{12}Cl_6H_{18.6}N_2O_{4.3}Ca_2Zn_2$: C, 21.0; Ca, 11.7; Cl, 31.0; H, 3.0; N, 4.1; Zn, 19.1%, Found: C, 21.2; Ca, 11.8; H, 2.9; N, 3.9; Cl, 31.3; Zn, 19.3%. (The calcium content present in this complex comes from using hard water by mistake.) Conductivity data (10^{-3} M in DMF): Λ_M = 3.0 ohm^{-1}. IR (cm^{-1}) ν(NH) 3156; $\nu_{as}(COO^-)$ 1733, 1633; $\nu_s(COO^-)$ 1378; ν(C—O) 1310; δ(NH) 1548; ν(Zn—O) 510 cm^{-1}. Raman: $\nu_{as}(COO^-)$ 1734; $\nu_s(COO^-)$ 1440; δ(NH) 1545; ν(Zn—O) 517; ν(Zn—Cl) 375 cm^{-1}, ^{1}H NMR (d_6-DMSO/TMS, ppm), δ: 3.50 (d, H, Hα); 2.50 (m, 2H, Hβ); 2.04 (m, 2H, Hγ); 1.43 (m, 2H, Hδ); 3.25, 2.74 (m, 2H, Hε); 13.22 (s, 1H, NH), ESI-MS: *m/z*, 339.3 [CaZn(Hpa)Cl_3]$^+$; 306.0 [CaZn(Hpa)Cl_2]$^+$; 268.0 [CaZn(Hpa)Cl]$^+$; 170.0 [Ca(Hpa)] $^+$; 128.0 [(Hpa)]$^+$.

2.3.3. Trans-[$Zn_2(\mu\text{-}Ca)_2(Hpa)_2Cl_6$]

Calcium chloride (0.11 g, 1 mmol) in water (15 mL) was added to an aqueous solution containing zinc chloride (0.136 g, 1 mmol) and DL-H_2pa (0.129 g, 1 mmol; 25 mL). The resulting solution was stirred and heated gently for 5 h. Upon reducing the volume, white crystals were separated out. They were filtered off, washed with water and dried *in vacuo*. Yield: 76%. Anal. Calcd. for $C_{12}Cl_6H_{18}N_2$-$O_4Ca_2Zn_2$: C, 21.2; Ca, 11.8; Cl, 31.4; H, 2.7; N, 4.1; Zn, 19.3%, Found: C, 21.1; Ca, 11.7; Cl, 31.2; H, 2.6; N, 4.0; Zn, 19.3%. Conductivity data (10^{-3} M in DMF): Λ_M = 5.0 ohm^{-1}. IR (cm^{-1}) ν(NH) 3155; $\nu_{as}(COO^-)$ 1734, 1636; $\nu_s(COO^-)$ 1381; ν(C—O) 1313; δ(NH) 1550; ν(Zn—O) 515 cm^{-1}. Raman: $\nu_{as}(COO^-)$ 1736; $\nu_s(COO^-)$ 1442; δ(NH) 1544; ν(Zn—O) 520; ν(Zn—Cl) 379 cm^{-1}, ^{1}H NMR (d_6-DMSO/TMS, ppm), δ: 3.48 (d, H, Hα); 2.51 (m, 2H, Hβ); 2.05 (m, 2H, Hγ); 1.42 (m, 2H, Hδ); 3.26, 2.77 (m, 2H, Hε); 13.32 (s, 1H, NH), ESI-MS: *m/z*, 678.8 [$Ca_2Zn_2(Hpa)_2Cl_6$]$^+$; 339.7 [CaZn(Hpa)Cl_3]$^+$; 304.0 [CaZn(Hpa)Cl_2]$^+$; 269.0 [CaZn(Hpa)Cl]$^+$; 128.0 [(Hpa)]$^+$.

2.3.4. [Pd(Hpa)(bpy)]Cl·2H_2O

Solid [Pd(bpy)Cl_2] (0.166 g, 0.5 mmol) was added to DL-H_2pa (0.064 g, 0.5 mmol) in ethanol (8 mL) containing triethyl amine (0.05 g, 0.5 mmol). The mixture was stirred for 72 h. The yellow-beige precipitate was filtered off, washed with ethanol and air-dried. Yield: 45%. Anal. Calcd. for $C_{16}ClH_{22}N_3O_4Pd$: C, 41.6; H, 4.8; N, 9.1; Cl, 7.7; Pd, 23.0%, Found: C, 41.5; H, 4.4; N, 9.0; Cl, 7.6; Pd, 23.1%. Conductivity data (10^{-3} M in DMF):Λ_M = 97.0 ohm^{-1}. IR (cm^{-1}): ν(NH) 3106; $\nu_{as}(COO^-)$ 1659; $\nu_s(COO^-)$ 1411; ν(Pd—O) 521; ν(Pd—N) 471 cm^{-1}. Raman: $\nu_{as}(COO^-)$ 1598; $\nu_s(COO^-)$ 1402; δ(NH) 1560; ν(Pd—O) 529; ν(Pd—N) 450 cm^{-1}; ^{1}H NMR (d_6-DMSO/TMS, ppm), 3.73 (d, H, Hα); 2.50 (m, 2H, Hβ); 2.07 (m, 2H, Hγ); 1.30 (m, 2H, Hδ); 3.45, 3.10 (m, 2H, Hε); 13.19 (s, H, NH), ESI-MS: *m/z*, 816.7 {Pd(Hpa)(bpy)]$_2$Cl}$^+$, 780.7 {[Pd(bpy)(Hpa)]$_2$}$^+$, 390.0 [Pd(bpy)(Hpa)]$^+$, 263.0 [Pd(bpy)]$^+$.

2.3.5. [Pt(Hpa)(bpy)]Cl

Solid [Pt(bpy)Cl_2] (0.211 g, 0.5 mmol) was added to DL-H_2pa (0.064 g, 0.5 mmol) in methanol (10 mL) containing KOH (0.028 g, 0.5 mmol). The mixture was stirred for 72 h, upon which a yellow precipitate was obtained. It was separated out, washed with methanol and air-dried. Yield: 70%. Anal. Calcd. for $C_{16}ClH_{18}$-N_3O_2Pt: C, 37.3; H, 3.5; N, 8.2; Cl, 6.9%, Found: C, 37.4, H, 3.4 N, 8.4; Cl, 6.8%. Conductivity data (10^{-3} M in DMF): Λ_M = 91.0 ohm^{-1}. IR (cm^{-1}): ν(NH) 3106; $\nu_{as}(COO^-)$ 1659; $\nu_s(COO^-)$ 1419; ν(Pd—O) 521; ν(Pd—N) 471 cm^{-1}; Raman: $\nu_{as}(COO^-)$ 1608; $\nu_s(COO^-)$

1420; δ(NH) 1558; ν(Pt—O) 512; ν(Pt-N) 400 cm^{-1} cm^{-1}; ^{1}H NMR (d_6-DMSO/TMS, ppm), 3.73 (d, H, Hα); 2.35 (m, 2H, Hβ); 2.04 (m, 2H, Hγ); 1.62 (m, 2H, Hδ); 3.54 (m, 2H, Hε); 13.10 (s, H, NH), ESI-MS: *m/z*, 465.0 $[Pt(Hpa\text{-}1/2N_2)(bpy)]^+$, 419.0 $[Pt(bpy)(Hpa\text{-}H_2CO_2N)]^+$, 379.0 $[Pt(bpy)(Hpa–Hpa\text{-}H_6C_4O_2N)]^+$.

2.3.6. $[Pd(PPh_3)_2(pa)]$

A suspension of $[Pd(PPh_3)_2Cl_2]$ (0.175 g, 0.25 mmol) in CH_2Cl_2 (15 mL) was added to DL-H_2pa (0.032 g, 0.25 mmol). The reaction mixture was stirred under reflux for 48 h. The yellow precipitate was filtered off, washed with CH_2Cl_2 and air-dried. Yield: 50%. Anal. Calcd. for $C_{42}H_{37}NO_2P_2Pd$: C, 66.5; H, 5.1; N, 1.9; Pd, 14.0%, Found: C, 66.2; H, 4.9; N, 1.8; Pd, 13.8%. Conductivity data (10^{-3} M in DMF): Λ_M = 6.0 ohm^{-1}. IR (cm^{-1}): $\nu_{as}(COO^-)$ 1653; $\nu_s(COO^-)$ 1409; ν(Pd—O) 514 cm^{-1}; Raman: $\nu_{as}(COO^-)$ 1640; $\nu_s(COO^-)$ 1440; ν(Pd—O) 523; ν(Pd—N) 431; ν(Pd—P) 392 cm^{-1}; ^{1}H NMR (d_6-DMSO/TMS, ppm), ^{1}H NMR (d_6-DMSO/TMS, ppm), δ 3.41 (d, H, Hα); 2.48 (m, 2H, Hβ); 2.03 (m, 2H, Hγ); 1.44 (m, 2H, Hδ); 3.21, 2.70 (m, 2H, Hε), ESI-MS (*m/z*): 758.0 $[Pd(pa)(PPh_3)_2]^+$, 631.0 $[Pd(PPh_3)_2]^+$.

2.3.7. $[Pt(pa)(PPh_3)_2]\cdot CH_2Cl_2$

A similar procedure as for the $[Pd(PPh_3)_2(Hpa)]Cl$ was applied in using $[Pt(PPh_3)_2Cl_2]$ (0.197 g, 0.25 mmol) and bright yellow precipitate was obtained. Yield: 70%. Anal. Calcd. for $C_{43}Cl_2H_{41}NO_2P_2Pt$: C, 55.4; Cl, 3.8; H, 4.4; N, 1.5%, Found: C, 56.0; Cl, 3.6; H, 4.8; N, 1.4%. Conductivity data (10^{-3} M in DMF): Λ_M = 9.0 ohm^{-1}. IR (cm^{-1}): $\nu_{as}(COO^-)$ 1646; $\nu_s(COO^-)$ 1384; ν(Pt—O) 509 cm^{-1}; Raman: $\nu_{as}(COO^-)$ 1584; $\nu_s(COO^-)$ 1340; ν(Pt—O) 537; ν(Pt—N) 447; ν(Pt—P) 390 cm^{-1} ^{1}H NMR (d_6-DMSO/TMS, ppm), δ 3.43 (d, H, Hα); 2.50 (m, 2H, Hβ); 2.09 (m, 2H, Hγ); 1.46 (m, 2H, Hδ); 3.54 (m, 2H, Hε), ESI-MS (*m/z*): 847.0 $[Pt(pa)(PPh_3)_3]^+$, 719.0 $[Pt(PPh_3)_2]^+$, 457.0 $[Pt(PPh_3)]^+$.

2.4. Biological assay

Growth inhibition assay; ovarian cancer ascites, OV 90 cells were plated at 3000 cells/well in 96-well (100 μL/well) flat-bottomed microliter plates (Costar, Corning, NY). After 24 h incubation, the cells were exposed to different concentrations of each compound continuously for 5 days. Briefly, following drug treatment, the cells were fixed using 50 μL of cold trichloroacetic acid (50%) for 2 h at 4 °C, washed with water, stained with sulforhodamine B (SRB 0.4%) overnight at room temperature, rinsed with 1% acetic acid and allowed to dry overnight [10]. The resulting colored residue was dissolved in 200 μL Tris base (10 mM, pH 10.0) and optical density was recorded at 490 nm using a microplate reader ELx808 (BioTek Instruments). The results were analyzed by GraphPad Prism (GraphPad Software, Inc., San Diego, CA) and the sigmoidal dose response curve was used to determine 50% cell growth inhibitory concentration ($IC5_0$). Each point represents the average of two independent experiments performed in triplicate [10].

3. Results and discussion

The experimental section described the synthesis of new complexes of Zn(II), Pd(II) and Pt(II) with DL-piperidine-2-carboxylic (DL-H_2pa; Fig. 1). The elemental analyses of the complexes are in excellent agreement with the assigned formulae. The molar conductivities (Λ_M) in DMF at room temperature suggest all complexes to be non-electrolytes except for, [M(bpy)(Hpa)]Cl (M(II) = Pd, Pt), which appear to be 1:1 electrolytes [11,12].

White sheets, suitable for X-ray crystallography, of *trans*-$[Zn_2(\mu\text{-}Ca)_2(Hpa)_2Cl_6]$ were obtained from the addition of $ZnCl_2$ to DL-H_2pa in hard tap water used by mistake in the preparation.

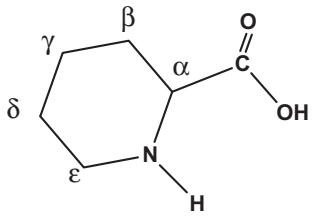

Fig. 1. Structure of H_2pa.

In addition, white crystals of the same complex, *trans*-$[Zn_2(\mu\text{-}Ca)_2(Hpa)_2Cl_6]$ were obtained from the addition of $CaCl_2$ to a mixture of $ZnCl_2$ and DL-H_2pa in distilled water. These crystals were mounted on the diffractometer and the unit cell dimensions and intensity data were measured at 150 K. The structure was solved by least-squares fit of the angular setting of strong reflections based on F^2. The relevant crystal data and experimental conditions along with the final parameters are summarized in Table 1.

3.1. Vibrational spectra

The characteristic IR and Raman bands and vibrational assignments observed for DL-piperidine-2-carboxylic acid (DL-H_2pa) complexes are reported in the experimental section. The spectral data of DL-H_2pa support its Zwitterionic form, similar to common amino acids (Scheme 1) [3,13]. This conclusion is supported by the presence of the ν_{as}(COO) and ν_a(COO) stretching modes at 1617 and 1397 cm^{-1}, respectively [3,13]. The nature of the coordination of the carboxylate groups have been classified on the basis of the difference ($\Delta\nu$) in the positions of the ν_{as}(COO) and ν_s(COO) bands [3,13–16]. In monodentate complexes, the ($\Delta\nu$) values are much greater than those in the ionic complexes. In chelating complexes the ($\Delta\nu$) values are significantly lower than the ionic values; and the ($\Delta\nu$) values for bridging complexes are greater than those of chelating (bidentate) complexes, and close to the ionic values.

In the reported complexes, the separation between the two vibrational bands $\{\Delta\nu = \nu_{as}(COO^-) - \nu_s(COO^-) > 220\ cm^{-1}\}$ is

Table 1
Crystal data and structure refinement for $C_6H_{10}CaCl_3NO_2Zn$ (using hard water).

Empirical formula	$C_6H_{10}CaCl_3NO_2Zn$
Formula weight	339.95
Temperature	150 K
Wavelength	1.54178 Å
Crystal system	Triclinic
Space group	P1
Unit cell dimensions	a = 7.5291(10) Å α = 87.489(6)°
	b = 7.7410(10) Å β = 77.799(7)°
	c = 10.8126(14) Å γ = 87.794(8)°
Volume	615.09(14) Å^3
Z	2
Density (calculated)	1.835 g/cm^3
Absorption coefficient	12.238 mm^{-1}
$F(000)$	340
Crystal size	0.06 × 0.04 × 0.02 mm
Theta range for data collection	5.72–69.95°
Index ranges	$-8 \leqslant h \leqslant 6$, $-8 \leqslant k \leqslant 9$, $-13 \leqslant \ell \leqslant 13$
Reflections collected	7665
Independent reflections	2202 [R_{int} = 0.067]
Absorption correction	Semi-empirical from equivalents
Max. and min. transmission	0.7829 and 0.5324
Refinement method	Full-matrix least-squares on F^2
Data/restraints/parameters	2202/0/131
Goodness-of-fit on F^2	1.091
Final R indices [I > 2sigma(I)]	R_1 = 0.0684, wR_2 = 0.1988
R indices (all data)	R_1 = 0.0731, wR_2 = 0.2032
Largest diff. peak and hole	1.092 and −0.890 e/Å^3

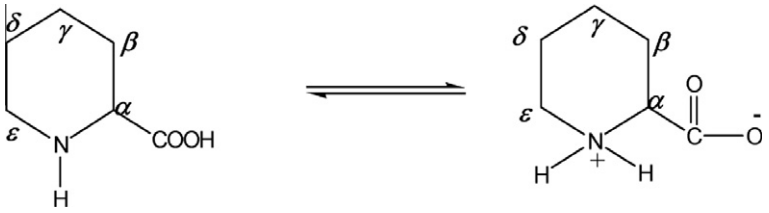

Scheme 1. Zwitter-ionic form of H_2pa.

greater than that of the free DL-H_2pa, indicating monodentate coordination of the carboxylate group [3,16,17]. Moreover, the carbonyl oxygen does not play any role in coordination, as no bands near 1700 cm^{-1} are observed [18]. The bands at 3140 and 1570 cm^{-1} arise from ν(NH) and δ(NH) vibrations, respectively and, as expected, these bands are shifted to lower wavenumber upon complex formation [3,4,15]. Raman and IR spectral data suggest N,O-mononegative bidentate coordination of DL-piperidine-2-carboxylate anion (Hpa^-) (Fig. 2), except in case of *trans*-[$Zn_2(\mu\text{-}Ca)_2(Hpa)_2Cl_6$] and [$M(PPh_3)_2(pa)$] (M(II) = Pd, Pt) complexes (Fig. 3). In the complexes, [$M(PPh_3)_2(pa)$] (M(II) = Pd, Pt), bands at 3140 and 1570 cm^{-1} in the free ligand due to ν(NH) and δ(NH) stretches are missing, while that arising from ν(C—N) is shifted to lower wavenumber [19,20]. The same feature have been reported in the X-ray crystal structures of [Au(Gly–Gly–His-H_{-2})]Cl and [Pd(Gly–Gly–His-H_{-2})], in which the terminal NH_2 and two deprotonated amide nitrogens are involved in coordination. Moreover, the potentiometric measurements of Pd(II) against Gly–Gly–His peptide support the deprotonation of pyrrole nitrogen center at pKa 8.63, which further confirmed by ^{1}H NMR spectroscopy [21]. These observations support the coordination of pa^{2-} *via* the deprotonated carboxylato oxygen and deprotonated cyclic nitrogen centers in a binegative manner.

On the other hand, the dimeric complex, *trans*-[$Zn_2(\mu\text{-}Ca)_2(Hpa)_2Cl_6$], illustrates two coordination manners of Hpa^-, since the $\Delta\nu$ value is slightly smaller than that of free H_2pa, i.e., the

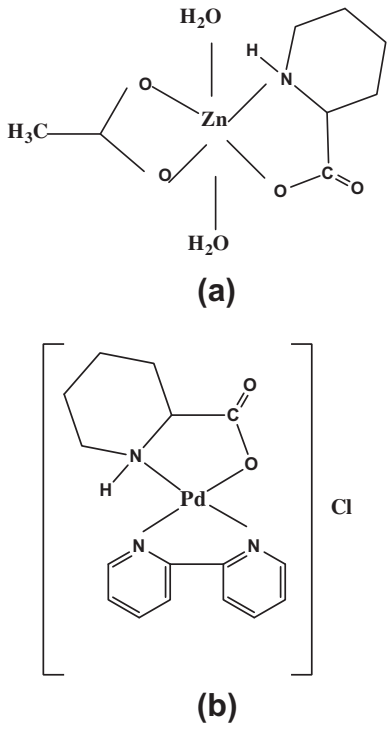

Fig. 2. Structures of [Zn(Hpa)(AcO)$(H_2O)_2$] (a) and [Pd(Hpa)(bpy)]Cl (b).

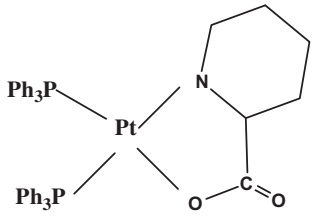

Fig. 3. Structure of [$Pt(pa)(PPh_3)_2$].

two Ca(II) ions seem to connect two carboxylato oxygen atoms in a bridging manner. The IR and Raman spectra show strong bands near 1735 cm^{-1} that may be assigned to ν(C=O) stretches, indicating that the ligand is linked *via* its carbonyl oxygen atom to Zn(II) [5,6,18]. This conclusion is further supported by the results obtained from the X-ray diffraction. The same behavior has been observed for [$CdCl_2$(Hpipe-3)] (Hpipe-3 = piperidine-3-carboxylic acid) [22].

As expected, the presence of coordinated PPh_3 in the [$M(PPh_3)_2(pa)$] (M(II) = Pd, Pt) complexes is indicated by strong bands near 1100 and 755 cm^{-1} due to ν(P—C) and δ(CCH) vibrations, respectively [23,24]. Also, the IR bands near 840, 750 and 725 cm^{-1} in the [M(bpy)(Hpa)]Cl (M(II) = Pd, Pt) complexes, are due to bpy stretching vibrations [25]. These bands are at higher wavenumbers compared with those for the free bpy ligand indicating the coordination to the central metal ions [26].

Finally, the Raman spectra of the complexes show several bands near 500, 420 and 281 cm^{-1} attributable to ν(M—O), ν(M—N) and ν(Zn—Cl) stretches, respectively [3,5,6,23].

3.2. NMR spectra

The ^{1}H NMR spectra of the reported complexes provide some information on the coordination mode and chelate ring conformation that DL-H_2pa ligand adopts. The ^{1}H NMR data for the free DL-H_2pa ligand and some of its complexes in DMSO-d_6 are given in the experimental section; they are in a good agreement with previously reported data [3]. On coordination of NH and COO^- groups, the protons attached to carbon atoms (Cα) become more deshielded than the NH in the Zwitterion because of the donation of electron pairs to the metal ion [3]. In the ^{1}H NMR spectra of the complexes, the proton bound to the nitrogen atom (NH) is clearly shown as a broad signal at δ13.10–13.22 ppm. The two doublets at δ 3.41–3.73 ppm region are assigned to Hα, while those at δ 3.20–3.54 ppm which appear as two multiplets overlapped by two quartets, respectively, are due to the two Hε protons. The multiplets at δ2.35–2.51, 2.03–2.09 and 1.30–1.62 ppm region are attributed to the Hβ, Hγ, Hδ protons, respectively. The upfield shift of the NH and Hα signals compared to that in the free ligand (Zwitterion) supports the coordination of DL-H_2pa to the metal ion through the NH and carboxylate oxygen centers [3,27,28]. In the ^{1}H NMR spectra of, the [$M(PPh_3)_2(pa)$] (M(II) = Pd, Pt) complexes, the NH proton signal is missing supporting the coordination of pa^{2-} through the

deprotonated cyclic nitrogen and the deprotonated carboxylate oxygen atoms [21].

The ^{1}H NMR spectra of the [M(bpy)(Hpa)]Cl and [M(PPh_3)$_2$(pa)] (M(II) = Pd, Pt) complexes show complicated multiplets in the δ 7.6–8.4 and 7.2–7.8 ppm regions, which are assigned to bpy and PPh_3 protons, respectively. The bpy and PPh_3 protons show upfield shifts in comparison to those of [M(bpy)Cl_2] and [M(PPh_3)Cl_2]. This observation is interpreted in terms of strong binding of Hpa^- or pa^{-2} to M(II) as compared to binding of chloride ion [3,27].

The ^{31}P NMR spectra of the [M(PPh_3)$_2$(pa)] (M(II) = Pd, Pt) complexes in DMSO-d6 display two sharp signals near δ 14.15 and 16.00 ppm, indicating the presence of the two PPh_3 groups in a *cis*-configuration [29].

3.3. Electronic spectra

The electronic spectra of the complexes were recorded in DMSO in the 200–800 nm range. The electronic spectra of the diamagnetic [M(bpy)(Hpa)]Cl and [M(PPh_3)$_2$(ap)] (M(II) = Pd, Pt) complexes show bands near 470 and 335 nm due to $^1A_{1g} \rightarrow {}^1B_{1g}$ and $^1A_{1g} \rightarrow {}^1E_{1g}$ transitions in a square-planar configuration [3,19,30]. The absorption band near 375 nm is assigned to combination of charge-transfer transitions from the M(II) d-orbital to the π^*-orbital of bpy or PPh_3 [31].

3.4. Mass spectra

Mass spectra of the complexes are reported in the experimental section and their molecular ion peaks are in agreement with their assigned formulae. The mass spectrum of [Zn(Hpa)(AcO)(H_2O)$_2$] shows fragmentation patterns corresponding to the successive degradation of the complex. The first peak at *m/z* 286.0 with 20% abundance represents the molecular ion (Calcd. 288.5). The peaks at 256.0 and 194.0 correspond to [Zn(pa)(AcO)]$^+$ and [Zn(pa)]$^+$ fragments, respectively. The mass spectrum of [Zn_2(μ-Ca)$_2$(Hpa)$_2Cl_6$] shows a peak at *m/z* 339.3 (Calcd. 340.0), in agreement with the molecular ion of the complex, [ZnCa(Hpa)Cl_3]$^+$, with 7.6% abundance. There are signals which represent stepwise loss of Cl fragments; [ZnCa(Hpa)Cl_2]$^+$ (Calcd. 304.5), [ZnCa(Hpa)Cl]$^+$ (Calcd. 269.0) and [Ca(Hpa)]$^+$ (Calcd. 168.0) [3,32]. The mass spectrum of [Pd(bpy)(Hpa)]Cl displays a signal at *m/z* 816.7 (Calcd. 816.3) with 100% abundance, in agreement with the dimeric molecular ion of the complex, {[Pd(bpy)(Hpa)]$_2$Cl}$^+$. The fragmentation patterns indicate formation of the fragments, {[Pd(bpy)(Hpa)]$_2$}$^+$ at 780.7 (Calcd. 780.8), [Pd(bpy)(Hpa)]$^+$ at 390.0 (Calcd. 390.4) and [Pd(bpy)]$^+$ at 264.0 (Calcd. 262.4) [33,34].

The mass spectrum of [Pt(bpy)(Hpa)]Cl shows a signal at *m/z* 465.0 (Calcd. 465.0) with 100% abundance, corresponding to the molecular ion of the complex, [Pt(bpy)(Hpa-N)]$^+$. The spectrum exhibits two more peaks at 419.0 and 379.0 corresponding to [Pt(bpy)(pa-CH_2NO_2)]$^+$ (Calcd. 419.0) and [Pt(bpy)(pa-$C_4H_4NO_2$)]$^+$ (Calcd. 379.0) fragments [30].

The mass spectrum of the [Pd(PPh_3)$_2$(pa)] complex shows first the molecular ion peak at *m/z* 758.0 (Calcd. 757.4) with 100% abundance, in agreement with the molecular ion, [Pd (PPh_3)$_2$(pa)]$^+$. The fragmentation patterns indicate the loss of pa, [Pd(PPh_3)$_2$]$^+$ at 631 (Calcd. 630.4) [8,30]. The mass spectrum of [Pt(pa)(PPh_3)$_2$] exhibits the first signal at *m/z* 846.0 (Calcd. 846.0) corresponding to [Pt(pa)(PPh_3)$_2$]$^+$ with two more signals at 719.0 (Calcd. 719.0) and 457.0 (Calcd. 457.0) corresponding to [Pt(PPh_3)$_2$]$^+$ and [Pt(PPh_3)]$^+$fragments, respectively [8,30].

3.5. Thermal measurements

The thermal stability and degradation behavior of some of the reported complexes were studied using the thermogravimetric (TG) technique. The complexes, [Zn(Hpa)(AcO)(H_2O)$_2$] and [Zn_2(μ-Ca)$_2$(Hpa)$_2Cl_6$]·1/3H_2O show endothermic behavior with mass losses between 190 and 290 °C, and 90 and 130 °C, respectively [31–33]. The percentages of mass loss for the two complexes in these decompositions are in good agreement with the values which are calculated by assuming that initially two molecules and then a third molecule of water are released. The dehydration temperatures suggest that these are coordinated and hydrated water, respectively [4,31].

The thermogram of [Zn(Hpa)(AcO)(H_2O)$_2$], shows three endothermic TG inflections in the 192–294, 295–362 and 363–503 °C regions. These weight losses may arise from the release of coordinated water molecules and acetate (AcO) (Calcd. 32.9, Found 33.4), C_2H_9N fragment (Calcd. 16.3, Found 17.0%) and an HCOH fragment (Calcd. 10.0, Found 9.8%), leaving a residue of zinc oxide and carbide (28.25%). The thermogram of [Zn_2(μ-Ca)$_2$(Hpa)$_2Cl_6$]·1/3H_2O, is characterized by four weight losses in the 93–128, 276–391, 392–517 and 587–796 °C regions. These weight losses are due to the elimination of hydrated water (Calcd. 0.9, Found 0.9%) [28], two Cl_2 and 1/2N_2 (Calcd. 22.7, Found 22.3%), 1/2N_2 and H_2 (Calcd. 2.3, Found 2.7%) and two C_6H_9Cl and CaO (Calcd. 42.1, Found 42.5%) fragments, respectively, leaving a mixture of CaO and two ZnO residues at 800 °C (27.8%) [6,22]. The TG thermogram of [Pt(bpy)(Hpa)]Cl shows the first endothermic weight loss step between 340 and 437 °C, corresponding to the release of 1/2Cl_2, 1/2 N_2 and HCOH fragments (Calcd. 16.8, Found 16.4%). The second decomposition step occurs between 510 and 677 °C, this weight loss is attributed the loss of ½ bpy and C_5H_{10} fragments (Calcd. 28.3, Found 28.6%), leaving PtO and carbide residue representing (52.9%). In some reported transition metal complexes, the thermal decomposition residue is mainly metal or metal oxide, but in the presence of non-stoichiometric oxide, unburned carbon or nitrogen is observed [33].

The thermal decomposition of the complex [Pd(PPh_3)$_2$(pa)], shows two TG inflections in the ranges of 184–250 and 251–350 °C. The exothermic weight losses may arise from the release of a fragment (Calcd. 11.2, Found 11.7%), and PPh_3 and three phenyl (Ph; C_6H_5) fragments (Calcd. 65.0, Found 65.5), respectively, leaving a PdO residue (16.2%) [33].

The TG thermogram of the complex [Pt(pa)(PPh_3)$_2$]·CH_2Cl_2, displays three TG weight losses in the ranges 188–251 °C, 252–346 and 413–537 °C. The first exothermic weight loss may arise from the release of dichloromethane and three Ph fragments (Calcd. 33.8, Found 33.9%). The second one is due to the loss of one P and C_6H_9NO fragments (Calcd. 15.4, Found 15.5%) while the third is indicating the loss of a PPh fragment (Calcd. 11.6, Found 12.2%), leaving a PtO residue (22.7%) [6].

3.6. X-ray crystallography

White sheets, suitable for X-ray crystallography of *trans*-[Zn_2(μ-Ca)$_2$(Hpa)$_2Cl_6$], obtained from the addition of $ZnCl_2$ to H_2pa in presence of $CaCl_2$ (in distilled water) or hard tap water (as a source of Ca^{2+}) by mistake in the preparation. These crystals were shown to crystallize in a triclinic lattice with space group symmetry P1. The crystal data and structure refinement details for these complexes are identical and given in Table 1 (Table 1 Supplementary data).

The structure of the dimeric, *trans*-[Zn_2(μ-Ca)$_2$(Hpa)$_2Cl_6$] complex with the atomic labeling is shown in Fig. 4 (X-ray obtained from the use of $CaCl_2$ in distilled water are present in Supplementary data). Selected bond angles (°) and bond lengths (Å) are listed in Table 2. Each one of the two zinc(II) ion is four coordinated in the center of tetrahedral geometry, ligated by one carbonyl oxygen of carboxylate group and three chloride ions. The bond lengths of Zn—O(2), Zn—Cl(1), Zn—Cl(2) and Zn—Cl(3) are 1.997(4),

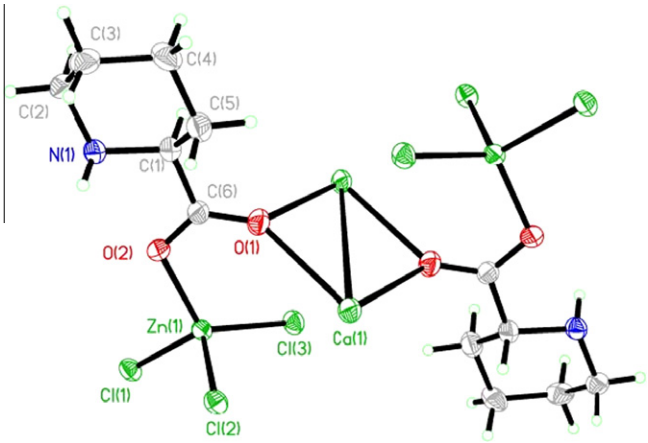

Fig. 4. X-ray crystal structure of *trans*-[$Zn_2(\mu\text{-}Ca)_2(Hpa)_2Cl_6$].

2.2768(15), 2.2745(14) and 2.2672(15) Å, similar to those of the corresponding bonds in [M(HPA)X_2] (M(II) = Zn, Cd; HPA = piperidine-2-carboxylic acid, piperidine-3-carboxylic acid, piperidine-4-carboxylic acid; X = Cl, Br) [4,6]. The bond length of C(6)—O(2), 1.268(8) Å is longer than C(6)—O(1), 1.236(7) Å, as reported for piperidine carboxylate complexes [6]. The two $ZnCl_3$ are *trans* to each other with O(2)—Zn—Cl(1), O(2)—Zn—Cl(2), O(2)—Zn—Cl(3), Cl(1)—Zn—Cl(2), Cl(1)—Zn—Cl(3) and Cl(2)—Zn—Cl(3) bite angles of 103.11(14)°, 108.33(15)°, 119.71(14)°, 109.16(6)°, 108.51(6)° and 107.67(6)°, respectively.

In this complex, two carboxyl oxygen atoms from two Hpa^- groups are bridged by two calcium atoms. The structure of this complex consists of two $Zn(Hpa^-)Cl_3$ units bridged by two calcium atoms. The bond lengths of Ca(1)—O(1) and Ca(2)—O(1) are 2.698(4) and 2.742(4) Å, longer than that of Zn—O(2) (1.997(4) Å). The bond angles of O(1)—Ca(1)—O(1a) and Ca(1)—O(1)—Ca(1a) are 89.34(13)° and 90.66(13)°, respectively, similar to the data observed for the bromide-bridged complex [Cd(HPA)Br_2] [4]. The strong coordination of Zn(II) to the two oxygen atom O(2), compared to that of Ca(II) to O(1) may be attributed to the high basicity of O(2) compared to O(1) [4,5,35].

In the crystal structure, the complex molecules form hydrogen bonded dimers *via* the nitrogen, N(1), and chlorine, Cl(1), atoms of a symmetry related molecule. Table 3 shows the bond lengths and bond angles related to the hydrogen bonding of the dimeric complex.

3.7. Anticancer activity

Cisplatin is considered to be one of the best known small metal-containing drug molecules. It acts as anticancer agent for several human cancers, particularly, testicular and ovarian cancers [19,36]. Generally, the side effects, especially nephrotoxicity, limit its widespread use in high doses [37]. The need to develop new complexes with reduced nephrotoxicity and higher activity has stimulated the synthesis of many new complexes. Over the past years, a renewed interest in Zn(II), Pd(II) and Pt(II) complexes as potential anticancer agents has developed in our laboratory [3,19,30,33,36,38].

Piperidine-2-carboxylic acid (DL-H_2pa) and its complexes [Pd(Hpa)(pa)]Cl, [Pd(pa)(H_2O)$_2$]Cl, [Pd(pa)(bpy)]Cl, [Pd(pa)(phen)Cl] and [Pd(pa)(pyq)Cl] have been tested as growth inhibitors against *Ehrlich ascites* tumor cells (EAC) in Swiss albino mice and were found to exhibit remarkable growth inhibitor activities [3].

The goal of this study was to develop new simple and mixed ligand complexes of piperidine-2-carboxylic acid (containing N and P bases) with high efficacy against cancer cells. The *in vitro* anticancer activity of the free DL-H_2pa and its complexes; *trans*-[$Zn_2(\mu\text{-}Ca)_2(Hpa)_2Cl_6$], [Pd(bpy)(Hpa)]Cl and [M(pa)(PPh_3)$_2$] (M(II) = Pd, Pt) were tested against the serous ovarian cancer ascites, OV 90 cell line in comparison to *cis*-platin as a reference (Table 4). The complex, [Pt(PPh_3)$_2$(pa)] exhibits the highest growth inhibitor activity with mean IC50 value of 43.13 μM. It is generally accepted that binding of *cis*-platin to genomic DNA (gDNA) in the cell nucleus is the main event responsible for its antitumor properties [39].

Table 2
Selected bond lenghts (Å) and bond angles (°) for $C_6H_{10}CaCl_3NO_2Zn$.

Bond lenghts (Å)		Bond angles (°)	
Zn(1)—O(2)	1.997(4)	O(2)—ZN1—CL3	119.71(14)
Zn(1)—Cl(3)	2.2672(15)	O(2)—ZN1—CL2	108.33(15)
Zn(1)—Cl(2)	2.2745(14)	CL3—ZN1—CL2	107.67(6)
Zn(1)—Cl(1)	2.2768(15)	O(2)—ZN1—CL1	103.11(14)
Zn(1)—Ca(1)	3.7414(15)	CL3—ZN1—CL1	108.51(6)
Ca(1)—O(1)	2.698(4)	CL2—ZN1—CL1	109.16(6)
Ca(1)—O(1)#1	2.742(4)	O(2)—ZN1—CA1	93.05(13)
Ca(1)—Cl(1)#2	3.1132(19)	CL3—ZN1—CA1	66.42(5)
Ca(1)—Cl(2)#3	3.1183(18)	CL2—ZN1—CA1	60.03(4)
Ca(1)—Cl(3)#1	3.258(2)	CL1—ZN1—CA1	163.09(5)
Ca(1)—Cl(2)	3.2663(19)	O(1)—CA1—O(1)#1	89.34(13)
Ca(1)—Ca(1)#1	3.869(2)	O(1)—CA1—CL1#2	161.57(13)
Cl(1)—Ca(1)#4	3.1132(19)	O(1)#1—CA1—CL1#2	85.81(10)
Cl(2)—Ca(1)#3	3.1183(18)	O(1)—CA1—CL2#3	84.95(11)
Cl(3)—Ca(1)#1	3.258(2)	O(1)#1—CA1—CL2#3	148.57(12)
O(1)—C(6)	1.236(7)	CL1#2—CA1—CL2#3	108.14(5)
O(1)—Ca(1)#1	2.742(4)	O(1)—CA1—CL3#1	69.92(11)
O(2)—C(6)	1.268(8)	O(1)#1—CA1—CL3#1	66.24(11)
N(1)—C(1)	1.485(8)	CL1#2—CA1—CL3#1	123.46(5)
N(1)—C(2)	1.490(8)	CL2#3—CA1—CL3#1	82.83(5)
C(1)—C(5)	1.501(10)	O(1)#1—CA1—CL2	129.73(11)
C(1)—C(6)	1.516(9)	O(1)—CA1—ZN1	48.99(11)
C(2)—C(3)	1.494(11)	O(1)#1—CA1—ZN1	99.75(10)
C(3)—C(4)	1.515(11)	CL1#2—CA1—ZN1	114.45(5)
C(4)—C(5)	1.524(11)	CL2#3—CA1—ZN1	99.60(4)
		CL3#1—CA1—ZN1	117.97(4)
		O(1)—CA1—CA1#1	45.13(9)
		O(1)#1—CA1—CA1#1	44.21(9)
		CL1#2—CA1—CA1#1	127.58(6)
		CL2#3—CA1—CA1#1	122.91(6)
		CL3#1—CA1-CA1#1	58.33(4)
		CL2—CA1—CA1#1	107.36(5)
		ZN1—CA1—CA1#1	70.27(4)
		ZN1—CL1—CA1#4	97.59(6)
		ZN1—CL2—CA1#3	123.34(6)
		ZN1—CL2—CA1	82.87(5)
		CA1#3—CL2—CA1	101.05(5)
		ZN1—CL3—CA1#1	103.46(6)
		C(6)—O(1)—CA1	140.7(4)
		C(6)—O(1)—CA1#1	125.3(4)
		CA1—O(1)—CA1#1	90.66(13)
		C(6)—O(2)—ZN1	111.4(4)
		C(1)—N(1)—C(2)	113.3(5)
		N(1)—C(1)—C(5)	110.8(5)
		N(1)—C(1)-C(6)	110.5(5)
		C(5)—C(1)—C(6)	114.7(5)
		N(1)—C(2)—C(3)	111.8(5)
		C(2)—C(3)—C(4)	110.3(6)
		C(3)—C(4)—C(5)	110.7(6)
		C(1)—C(5)—C(4)	111.8(6)
		O(1)—C(6)—O(2)	124.5(6)
		O(1)—C(6)—C(1)	117.8(6)
		O(2)—C(6)—C(1)	117.6(5)

Table 3
Bond lengths (Å) and angles (°) related to the hydrogen bonding for $C_6H_{10}CaCl_3NO_2Zn$.

D—H	*A*	*d*(D—H)	*d*(H···A)	*d*(D···A)	<DHA
N(1)—H(1A)	CL1#5	0.90(8)	2.39(8)	3.266(5)	163(7)

Symmetry transformations used to generate equivalent atoms.
#1 $-x, -y, -z$ #2 $x-1, y, z$ #3 $-x, -y+1, -z$.
#4 $x+1, y, z$ #5 $-x+1, -y+1, -z$.

Table 4
Anticancer activity of H_2pa and its complexes against the human ovarian cancer ascites, OV 90 cell line.

Compound	IC_{50} (μM)
H_2pa	>100
trans-$[Zn_2(\mu\text{-}Ca)_2(Hpa)_2Cl_6]$	>100
[Pd(bpy)(Hpa)]Cl	>100
$[Pd(pa)(PPh_3)_2]$	>100
$[Pt(pa)(PPh_3)_2]$	43.13
Cis-platin	31.06

Thus, the damage induced upon binding of cisplatin to gDNA may inhibit transcription, and/or DNA replication mechanisms. Subsequently, these alterations in DNA processing would trigger cytotoxic processes that lead to cancer cell death. The activity of $[Pt(pa)(PPh_3)_2]$ complex may be due to its square-planar geometry, chelation of pa^{2-} in binegative (O and N) manner as well as the nature and position of the second ligand (*cis*-$(PPh_3)_2$) [3,19,38]. An important property of Pt(II) complexes is the fact that Pt-ligand bonds (Pt—P, Pt—N, Pt—O), which have thermodynamic strength of a typical coordination bond, is much weaker than C—C, C—N or C—O covalent bonds. However, the ligand exchanges behavior in Pt complexes are quite slow, which gives them high kinetic stability. Thus, ligand exchange reactions take place in minutes to days, rather than microsecond to second as in case of Pd(II) complexes [40]. Also, the kinetic *trans* effect is responsible for ligands exchange reactions; i.e., donor atoms located *trans* to other donors with strong *trans* effect are more rapidly substituted than ligands in *cis* positions [40]. On the other hand, the low activity of the other complexes, *trans*-$[Zn_2(\mu\text{-}Ca)_2(Hpa)_2Cl_6]$, [Pd(Hpa)(bpy)]Cl and $[Pd(pa)(PPh_3)_2]$, may be due to the poor solubility (except in case of [Pd(Hpa)(bpy)]Cl, which is water soluble), difficulty in hydrolysis to be cationic or fast interaction with DNA under physiological conditions [40]. Furthermore, the presence of intermolecular hydrogen bonds, as indicated from the crystal structure of *trans*-$[Zn_2(\mu\text{-}Ca)_2(Hpa)_2Cl_6]$, may reduce its activity [41].

4. Conclusions

New complexes of DL-H_2pa have been prepared and characterized. DL-H_2pa acts as bidentate ligand, coordinating the metal atoms through the carboxyl oxygen and cyclic nitrogen atoms. The crystal structure of *trans*-$[Zn_2(\mu\text{-}Ca)_2(Hpa)_2Cl_6]$ has been determined by X-ray diffraction. In which, each one of the two zinc atoms occupies tetrahedral geometry, ligates by carbonyl oxygen and three chlorine atoms. The other carboxyl oxygen atoms from two Hpa^- groups are bridged by two calcium atoms, i.e., there are two $Zn(Hpa^-)Cl_3$ units bridged by two calcium atoms. The free DL-H_2pa and its complexes; *trans*-$[Zn_2(\mu\text{-}Ca)_2(Hpa)_2Cl_6]$, [Pd(bpy)(Hpa)]Cl and $[M(pa)(PPh_3)_2]$ (M(II) = Pd, Pt) were tested against the human serous ovarian cancer ascites, OV 90 cell line. The complex, $[Pt(PPh_3)_2(pa)]$ exhibits the highest growth inhibitory activity with mean IC50 value of 43.13 μM.

Acknowledgements

We are grateful to Mr. Joel Poisson (Chemistry Department, McGill University, Montreal Canada) for running the NMR spectra, Dr. Kelly Akers (ProSpect Scientific inc., Ontario, Canada) and Dr. Morgan Thomas (Saskatchewan Structural Sciences Centre, University of Saskatchewan) for measuring the Raman spectra, and Mr. Nadim Saade (Chemistry Department, McGill University, Montreal, Canada) for obtaining the mass spectra.

Appendix A. Supplementary material

CCDC numbers: CCDC of the crystals obtained are 875432 and 875433 for *trans*-$[Zn_2(\mu\text{-}Ca)_2(Hpa)_2Cl_6]$.

Supplementary data associated with this article can be found, in the online version, at http://dx.doi.org/10.1016/j.molstruc.2012.09.045.

References

[1] S. Kallstrom, R. Leino, Bioorg. Med. Chem. 16 (2008) 601.
[2] C. Rebello, M.G. Ram Reddy, Indian J. Chem. 24A (1985) 765.
[3] S.I. Mostafa, Transition Met. Chem. 32 (2007) 769.
[4] Y. Inomata, Y. Arai, T. Yamakoshi, F. Scott Howell, Inorg. Biochem. 98 (2004) 2149.
[5] Y. Inomata, M. Ando, F. Scott Howell, J. Mol. Struct. 616 (2002) 201.
[6] Y. Inomata, K. Sasaki, H. Umehara, F. Scott Howell, Inorg. Chim. Acta 313 (2001) 95.
[7] H.M. Haendler, Acta Cryst. C41 (1985) 690.
[8] W.P. Griffith, S.I. Mostafa, Polyhedron 11 (1992) 871.
[9] R.C. Cookson, D.W. Jones, J. Chem. Soc. (1965) 1881.
[10] P. Skehan, R. Storeng, D. Scudiero, J. Natl. Cancer Inst. 82 (1990) 1107.
[11] W. Geary, Coord. Chem. Rev. 7 (1981) 81.
[12] A. Kula, J. Therm. Anal. Calorim. 68 (2002) 957.
[13] A. Szoecsik, L. Nagy, M. Scopelliti, A. Deak, L. Pellerito, K. Hegetschweiler, J. Organomet. Chem. 690 (2005) 2280.
[14] C.C. Wagner, E.J. Baran, Acta Pharm. Bonaerense 21 (2002) 287.
[15] P.I. Girginova, F.A. Almeida Paz, H.I.S. Nogueira, N.J.O. Silva, V.S. Amaral, J. Klinowski, T. Trindade, Polyhedron 24 (2005) 563.
[16] K. Nakamoto, Infrared and Raman Spectra of Inorganic and Coordination Compounds, Part B, fifth ed., Wiley, New York, 1997. p. 60.
[17] G. Eng, X. Song, A. Zapata, A.C. de Dios, L. Casabiana, R.D. Pike, J. Organomet. Chem. 692 (2007) 1398.
[18] M.A. Goher, M.A. Abu-Youssef, F.A. Mautner, Polyhedron 15 (1996) 453.
[19] S.I. Mostafa, F.A. Badria, Metal-Based Drugs (2008) 1–7, http://dx.doi.org/10.1155/ 2008/723634.
[20] S.I. Mostafa, M.A. Kabil, E.M. Saad, A.A. El-Asmy, J. Coord. Chem. 59 (2006) 279.
[21] S.L. Best, T.K. Chattopadhyay, M.I. Djuran, R.A. Palmer, P.J. Sadler, I. Sóvágó, K. Varnagy, J. Chem. Soc. Dalton Trans. (1997) 2587.
[22] J. Yamada, Y. Inomata, T. Takeuchi, Inorg. Chim. Acta 249 (1996) 121.
[23] S.I. Mostafa, C. Papatriantafyllopoulou, S. Perlepes, N. Hadjiliadis, Bioinorg. Chem. Appl. doi:10.1155/2008/647873.
[24] A.G.de A. Fernandes, V.M. Deflon, E.J. de Souza, P.I.S. Maia, A.A. Batista, S.S. Lemos, U. Abram, J. Ellena, E.E. Castellano, Polyhedron 27 (2008) 2983.
[25] A.K. Boudalis, V. Nastopoulos, S.P. Perlepes, C.P. Raptopoulou, A. Terzis, Transition Met. Chem. 26 (2001) 276.
[26] S. Aruna, G. Shanmugam, Spectrochim. Acta 41A (1985) 531.
[27] V.X. Jin, J.D. Ranford, Inorg. Chim. Acta 304 (2000) 38.
[28] M.D. Couce, G. Faraglia, U. Russo, L. Sinellari, G. Valle, A. Furlani, V. Scarcia, New J. Chem. 21 (1997) 1103.
[29] M. Tamizh, K. Mereitter, K. Kirchner, B.R. Bhat, R. Karvembu, Polyhedron 28 (2009) 2157.
[30] S.I. Mostafa, J. Coord. Chem. 61 (2008) 1553.
[31] S.I. Mostafa, S.P. Perlepes, N. Hadjiliadis, Z. Naturforsch. 56b (2001) 394.
[32] A.M. Ouf, M.S. Ali, E.M. Saad, S.I. Mostafa, J. Mol. Struct. 973 (2010) 69.
[33] I. Gabr, H. El-Asmy, M. Emmam, S.I. Mostafa, Transition Met. Chem. 34 (2009) 409.
[34] A.M. Ouf, M.S. Ali, M.S. Soliman, A.M. El-Defrawy, S.I. Mostafa, J. Kor. Chem. Soc. 54 (2010) 402.
[35] S. El-Sayed, A.M. El-Hendawy, I.S. Butler, S.I. Mostafa, J. Mol. Struct., in press. http://dx.doi.org/10.1016/j.molstruc.2012.09.018.
[36] S. El-Sayed, B. Jean Claude, I. Butler, S. Mostafa, J. Mol. Struct. 1028 (2012) 208.
[37] F.P.T. Harmers, W.H. Gispen, J.P. Neijt, Eur. J. Cancer 27 (1991) 372.
[38] S.A. Elsayed, A.M. El-Hendawy, S.I. Mostafa, B.J. Jean-Claude, M. Todorova, Ian S. Butler, Bioinorg. Chem. Appl. 2010, 1-11. doi:10.1155/2010/149149.
[39] V. Cepeda, M.A. Fuertes, J. Castilla, C. Alonso, C. Quevedo, J.M. Pérez, Anti-Cancer Agents Med. Chem. 7 (2007) 3.
[40] I. Kostova, Recent Patents Anti-cancer Drug Discovery I (2006) 1.
[41] K.I. Goldberg, J. Valdes-Martinez, G. Espinosa-Perez, L.J. Ackerman, D.X. West, Polyhedron 18 (1999) 1177.